VIETNAM ACADEMY OF SCIENCE AND TECHNOLOGY

Vietnam Journal of MECHANICS

Volume 36 Number 1

ISSN 0866-7136

VN INDEX 12.666

1

2014

Vietnam Journal of Mechanics, VAST, Vol. 36, No. 1 (2014), pp. 13 – 25

CRACK DETECTION OF A BEAM-LIKE BRIDGE USING 3D MODE SHAPES

Nguyen Viet Khoa
Institute of Mechanics, VAST, 18 Hoang Quoc Viet, Hanoi, Vietnam
E-mail: nvkhoa@imech.ac.vn
Received May 02, 2013

Abstract. In this paper, mode shapes of a 3D cracked beam with a rectangular cross section are analyzed for crack detection. The influence of coupling mechanism between horizontal and vertical bending vibrations due to the 3D crack model on the mode shapes is investigated. Due to the coupling mechanism the mode shapes of a beam are twisted in space. They change from plane curves to space curves. This phenomenon can be used for crack detection. The existence of the crack can be detected when the mode shapes are space curves. Also, the mode shapes of a cracked beam bridge have distortions or sharp changes at the crack position. Therefore, the position of the crack can be determined as a position at which the mode shapes exhibit such distortions or sharp changes. Moreover, using the mode shapes in 3D crack model, a crack with depth as small as 1% of the beam height can be detected, while in previous studies using 2D crack model, distortions in the mode shapes caused by a small crack cannot be detected. These results are new and can be used for crack detection of a beam bridge. The stiffness matrix of a 3D cracked element obtained from fracture mechanics is presented and numerical simulations are provided in this paper.

Keywords: Crack, crack detection, 3D crack, bending effect.

1. INTRODUCTION

The existence of a crack in a structure will influence its dynamic characteristics such as natural frequencies and mode shapes. Therefore, information from the natural frequencies and mode shapes is useful for crack detection. The most important problem for analysing the vibration of a cracked beam is to model the local stiffness at the crack position. Chondros et al. [1] developed a continuous cracked beam vibration theory for the lateral vibration of cracked Euler-Bernoulli beams with single-edge or double-edge open cracks. The crack was modelled as being continuously flexible using the displacement field in the vicinity of the crack found in fracture mechanics. Lee et al. [2] studied the influence of a crack on natural frequencies and mode shapes of a beam. The stiffness matrix of the cracked beam is derived from a flexibility matrix calculated from fracture mechanics. Sadettin Orhan [3] investigated the influences of the depth and location of the crack on the natural frequency of a cracked beam. In this study, the flexibility matrix of

the crack was calculated by using the stress intensity factors based on the finite element method (FEM). A perturbation method and a transfer matrix approach were proposed by Gudmundson [4] to investigate the influence of small cracks on the natural frequencies of slender structures. Zhang et al. [5] presented a method using the transform matrix to calculate frequencies and mode shapes of a cracked cantilever beam. Some authors [6–9] modelled cracks as massless rotational springs, whose stiffness were obtained from fracture mechanics to study the natural frequencies and mode shapes of cracked beams. Recently, the author of this paper [10] presented a vibration based method for open and breathing crack detection of a beam bridge subjected to a moving vehicle. The stiffness matrix of a breathing cracked element was calculated from the stiffness matrix of the intact and open cracked element which was obtained from fracture mechanics.

Most of the researches model the beams as 1D and 2D structures for investigating pure longitudinal or bending vibrations, only few of the current works used the 3D beam model to study more complicated vibrations of the beams. The coupled bending and longitudinal vibration of a cracked rotor were studied by Papadopoulos et al. [11]. Coupled bending, longitudinal and torsional vibrations of a cracked rotor were investigated by Darpe et al. [12]. Saavedra et al. [13] investigated the frequency of forced vibration of a 3D cracked beam. In these works, the 12×12 stiffness matrices of a cracked element obtained from fracture mechanics were applied. However, in these works only forced vibrations were investigated while the influence of a 3D crack on the dynamic characteristics of a beam such as frequency and mode shape had not been considered and compared with that of the 1D and 2D beams.

From the above mentions, this paper analyses the influence of the 3D crack model on the dynamic characteristics of a beam bridge for crack detection purpose. The influence of the coupling mechanism between horizontal bending and vertical bending vibrations on the mode shapes of beam due to the 3D crack model is investigated. It is interesting to show that, while the mode shapes of the intact beam are plane curves, the mode shapes of the cracked beam are twisted in the 3D space and become space curves. Moreover, there are distortions or sharp changes in these mode shapes at the position of the crack. These distortions can be inspected visually with a very small crack by amplifying the mode shapes to an appropriate scale. In this study, the detection of a crack with depth as small as 1% of the beam height is illustrated. This result is new and can be applied for crack detection of a beam. The stiffness matrix of the beam obtained from the fracture mechanics and the numerical simulation are presented in this paper.

2. FREE VIBRATION OF AN INTACT BEAM IN FINITE ELEMENT METHOD

In this study, the bridge is considered as an Euler-Bernoulli uniform beam with a constant rectangular cross-section. The beam is divided by R elements in finite element analysis. The governing equation of undamped free vibration of the beam can be written following the finite element method as follows [14]

$$\mathbf{M}\ddot{\mathbf{d}} + \mathbf{K}\mathbf{d} = 0 \tag{1}$$

where **M**, **K** are structural mass and stiffness matrices; **d** is a column vector which denotes the displacement of the beam.

The solution of Eq. (1) can be found in the form of

$$\mathbf{d} = \varphi e^{i\omega t} \tag{2}$$

Here φ is the amplitude of the nodal displacement, ω is the natural frequency of the beam, and t is the time. Substituting Eq. (2) into Eq. (1), we have

$$\left[\mathbf{K} - \omega^2 \mathbf{M}\right] \varphi = 0 \tag{3}$$

or

$$\left[\mathbf{K} - \lambda \mathbf{M}\right] \varphi = 0 \tag{4}$$

where

$$\lambda = \omega^2 \tag{5}$$

Eq. (4) is called the eigenvalue equation. To have a non-zero solution for φ, the determinant of the matrix must be zero

$$\det\left[\mathbf{K} - \lambda \mathbf{M}\right] = \left|\mathbf{K} - \lambda \mathbf{M}\right| = 0 \tag{6}$$

N roots λ_1, λ_2,..., λ_N, called eigenvalues will be determined by solving this equation, where N is the number of DOFs. By substituting these eigenvalue λ_i back into the eigenvalue Eq. (4) and solving this equation the eigenvector φ will be obtained.

3. FINITE ELEMENT MODEL OF A CRACKED BEAM WITH RECTANGULAR CROSS SECTION

Considering a uniform beam bridge with rectangular cross section with a crack located at the distance L_c from the left end. Fig. 1 presents the model of 3D cracked element with 12 degrees of freedom. The element is loaded with shear forces P_2, P_3, P_8, P_9, bending moments P_4, P_5, P_{11}, P_{12}, axial forces P_1, P_7, and torsional moments P_4, P_{10}.

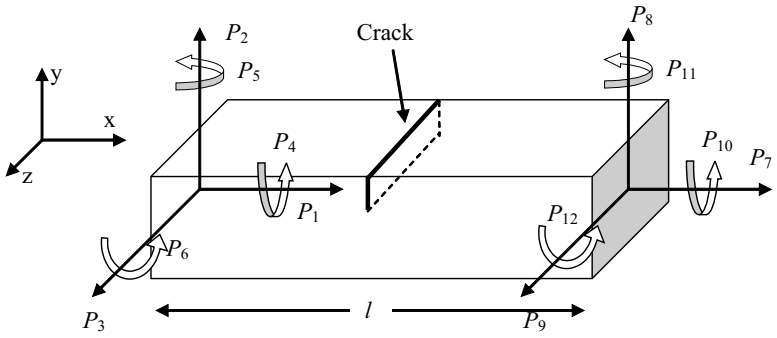

Fig. 1. Model of the cracked element

The stiffness matrix of a cracked element can be derived from the flexibility matrix as follows [12].

Using Castingliano's theorem, a component $\tilde{c}_{ij}$ of the total flexibility matrix $\tilde{C}$ is the sum of the flexibility coefficient of the intact element and the additional flexibility coefficient due to the crack

$$\tilde{c}_{ij} = \tilde{c}_{ij}^{(o)} + \tilde{c}_{ij}^{(1)} \tag{7}$$

where the flexibility coefficient of the intact element is

$$\tilde{c}_{ij}^{(0)} = \frac{\partial^2 W^{(0)}}{\partial P_i \partial P_j}; \quad i,j = 1,2,...,6 \tag{8}$$

and the additional flexibility coefficient is

$$\tilde{c}_{ij}^{(1)} = \frac{\partial^2 W^{(1)}}{\partial P_i \partial P_j}; \quad i,j = 1,2,...,6 \tag{9}$$

Here, $W^{(0)}$ is the strain energy of the uncracked element; $W^{(1)}$ is the strain energy due to the crack.

The elastic strain energy of the element can be obtained by considering the action of axial forces, shear forces, torsion and bending moments at the cross section of the crack as follows [12]

$$W^{(0)} = \frac{1}{2}\left[\frac{P_1^2 l}{AE} + \frac{\kappa P_2^2 l}{GA} + \frac{\kappa P_3^2 l}{GA} + \frac{P_2^2 l^3}{3EI_z} + \frac{P_6^2 l}{EI_z} + \frac{P_2 P_6 l^2}{3EI_z} + \frac{P_3^2 l^3}{3EI_y} + \frac{P_5^2 l}{EI_y} - \frac{P_3 P_5 l^2}{EI_y} + \frac{P_4^2}{GI_0}\right] \tag{10}$$

Where G is the modulus of rigidity, E is Young's modulus; A is the cross section area; I_y, I_z are the inertia moments of the cross section about y and z axes, respectively; I_0 is the polar moment of inertia of the cross section; κ is the shear coefficient.

The additional energy due to the crack of a rectangular element with thickness h and width b can be expressed as follows

$$W^{(1)} = \int_A \frac{1}{E'}\left[\left(\sum_1^6 K_{\mathrm{I}i}\right)^2 + \left(\sum_1^6 K_{\mathrm{II}i}\right)^2 + \mu\left(\sum_1^6 K_{\mathrm{III}i}\right)^2\right] dA \tag{11}$$

where $E' = \dfrac{E}{1-\nu^2}$ and μ=1+ν, and $K_{\mathrm{I}i}$, $K_{\mathrm{II}i}$, $K_{\mathrm{III}i}$ are stress intensity factors for opening type, sliding type and tearing type cracks, respectively; $i = 1,2,...,6$.

Stress intensity factors are obtained from reference [15]

$$\begin{aligned}
&K_{\mathrm{I}1} = \sigma_1\sqrt{\pi\alpha}F_1(\bar{\alpha}), \sigma_1 = \frac{P_1}{bh}, K_{\mathrm{I}5} = \sigma_5\sqrt{\pi\alpha}F_1(\bar{\alpha}), \sigma_5 = \frac{12P_5 z}{b^3 h},\\
&K_{\mathrm{I}6} = \sigma_6\sqrt{\pi\alpha}F_2(\bar{\alpha}), \sigma_6 = \frac{6P_6}{bh^2}, K_{\mathrm{I}2} = K_{\mathrm{I}3} = K_{\mathrm{I}4} = 0,\\
&K_{\mathrm{II}2} = \sigma_2\sqrt{\pi\alpha}F_{\mathrm{II}}(\bar{\alpha}), \sigma_2 = \frac{\kappa P_2}{bh}, K_{\mathrm{II}4} = \sigma_4\sqrt{\pi\alpha}F_{\mathrm{II}}(\bar{\alpha}), \sigma_4 = \frac{P_4}{bh},\\
&K_{\mathrm{II}1} = K_{\mathrm{II}3} = K_{\mathrm{II}5} = K_{\mathrm{II}6} = 0, K_{\mathrm{III}3} = \sigma_3\sqrt{\pi\alpha}F_{\mathrm{III}}(\bar{\alpha}), \sigma_3 = \frac{\kappa P_3}{bh}\\
&K_{\mathrm{III}4} = \sigma_{4\mathrm{III}}\sqrt{\pi\alpha}F_{\mathrm{III}}(\bar{\alpha}), \sigma_{4\mathrm{III}} = \frac{P_4}{bh}, K_{\mathrm{III}1} = K_{\mathrm{III}2} = K_{\mathrm{III}5} = K_{\mathrm{III}6} = 0
\end{aligned} \tag{12}$$

Here α is the crack depth variable, $\bar{\alpha} = \dfrac{\alpha}{h}$, and

$$
\begin{aligned}
F_1\left(\frac{\alpha}{h}\right) &= \sqrt{\frac{2h}{\pi\alpha}\tan\left(\frac{\pi\alpha}{2h}\right)}.\frac{0.752 + 2.02\left(\dfrac{\alpha}{h}\right) + 0.37\left(1 - \sin\dfrac{\pi\alpha}{2h}\right)^3}{\cos\dfrac{\pi\alpha}{2h}} \\
F_2\left(\frac{\alpha}{h}\right) &= \sqrt{\frac{2h}{\pi\alpha}\tan\left(\frac{\pi\alpha}{2h}\right)}.\frac{0.923 + 0.199\left(1 - \sin\dfrac{\pi\alpha}{2h}\right)^4}{\cos\dfrac{\pi\alpha}{2h}} \\
F_{\mathrm{II}}\left(\frac{\alpha}{h}\right) &= \left(1.122 - 0.561\left(\frac{\alpha}{h}\right) + 0.085\left(\frac{\alpha}{h}\right)^2 + 0.18\left(\frac{\alpha}{h}\right)^3\right) \Big/ \sqrt{1 - \frac{\alpha}{h}} \\
F_{\mathrm{III}}\left(\frac{\alpha}{h}\right) &= \sqrt{\frac{2h}{\pi\alpha}\tan\frac{\pi\alpha}{2h}}
\end{aligned}
\tag{13}
$$

The stiffness matrix of the cracked element is derived as follows [16]

$$\mathbf{K}_{\mathrm{c}} = \mathbf{T}^{\mathrm{T}}\tilde{\mathbf{C}}^{-1}\mathbf{T} \tag{14}$$

where $\mathbf{T}$ is the transformation matrix

$$
\mathbf{T} = \begin{bmatrix}
-1 & 0 & 0 & 0 & 0 & 0 & 1 & 0 & 0 & 0 & 0 & 0 \\
0 & -1 & 0 & 0 & 0 & -l & 0 & 1 & 0 & 0 & 0 & 0 \\
0 & 0 & -1 & 0 & l & 0 & 0 & 0 & 1 & 0 & 0 & 0 \\
0 & 0 & 0 & -1 & 0 & 0 & 0 & 0 & 0 & 1 & 0 & 0 \\
0 & 0 & 0 & 0 & -1 & 0 & 0 & 0 & 0 & 0 & 1 & 0 \\
0 & 0 & 0 & 0 & 0 & -1 & 0 & 0 & 0 & 0 & 0 & 1
\end{bmatrix}
\tag{15}
$$

where l is the length of the element. The stiffness and mass matrices for a 3D element without a crack are obtained from the finite element method as follows

$$
k_{\mathrm{e}} = \begin{bmatrix}
\frac{AE}{2a} & 0 & 0 & 0 & 0 & 0 & \frac{-AE}{2a} & 0 & 0 & 0 & 0 & 0 \\
 & \frac{3EI_z}{2a^3} & 0 & 0 & 0 & \frac{3EI_z}{2a^2} & 0 & \frac{-3EI_z}{2a^3} & 0 & 0 & 0 & \frac{3EI_z}{2a^2} \\
 & & \frac{3EI_y}{2a^3} & 0 & \frac{-3EI_y}{2a^2} & 0 & 0 & 0 & \frac{-3EI_y}{2a^3} & 0 & \frac{-3EI_y}{2a^2} & 0 \\
 & & & \frac{GI_0}{2a} & 0 & 0 & 0 & 0 & 0 & \frac{-GI_0}{2a} & 0 & 0 \\
 & & & & \frac{2EI_y}{a} & 0 & 0 & 0 & \frac{3EI_y}{2a^2} & 0 & \frac{EI_y}{a} & 0 \\
 & & & & & \frac{2EI_z}{a} & 0 & \frac{-3EI_z}{2a^2} & 0 & 0 & 0 & \frac{EI_z}{a} \\
 & & & & & & \frac{AE}{2a} & 0 & 0 & 0 & 0 & 0 \\
 & & & & & & & \frac{3EI_z}{2a^3} & 0 & 0 & 0 & \frac{-3EI_z}{2a^2} \\
 & & & sy. & & & & & \frac{3EI_y}{2a^3} & 0 & \frac{3EI_y}{2a^2} & 0 \\
 & & & & & & & & & \frac{GI_0}{2a} & 0 & 0 \\
 & & & & & & & & & & \frac{2EI_y}{a} & 0 \\
 & & & & & & & & & & & \frac{2EI_z}{a}
\end{bmatrix}
\tag{16}
$$

$$m_{\mathrm{e}} = \frac{\rho A a}{105}\begin{bmatrix} 70 & 0 & 0 & 0 & 0 & 0 & 35 & 0 & 0 & 0 & 0 & 0 \\ & 78 & 0 & 0 & 0 & 22a & 0 & 27 & 0 & 0 & 0 & -13a \\ & & 78 & 0 & -22a & 0 & 0 & 0 & 27 & 0 & 13a & 0 \\ & & & 70r_x^2 & 0 & 0 & 0 & 0 & 0 & -35r_x^2 & 0 & 0 \\ & & & & 8a^2 & 0 & 0 & 0 & -13a & 0 & -6a^2 & 0 \\ & & & & & 8a^2 & 0 & 13a & 0 & 0 & 0 & -6a^2 \\ & & & & & & 70 & 0 & 0 & 0 & 0 & 0 \\ & & & & & & & 78 & 0 & 0 & 0 & -22a \\ & & & & & & & & 78 & 0 & 22a & 0 \\ & & & sy. & & & & & & 70r_x^2 & 0 & 0 \\ & & & & & & & & & & 8a^2 & 0 \\ & & & & & & & & & & & 8a^2 \end{bmatrix} \quad (17)$$

Where $a = \dfrac{l}{2}$, $r_x = \dfrac{I_x}{a}$, and I_x, I_y, I_z are second moments of area (or moments of inertia) of the cross-section of the beam with respect to the x, y and z axes; I_0 is the polar moment of inertia of the cross section; E is the Young's modulus.

Finally, the global mass matrix $\mathbf{M}$ is assembled from the element mass matrices $\mathbf{m}_e$ and the global stiffness matrix $\mathbf{K}$ of the cracked beam is assembled from the element stiffness $\mathbf{k}_e$ and $\mathbf{k}_c$. By substituting these matrices $\mathbf{M}$ and $\mathbf{K}$ into Eqs. (4)-(6) and solving them, the eigenvalues and eigenvector of the cracked beam are obtained.

4. NUMERICAL SIMULATION AND DISCUSSIONS

A numerical example of a beam like bridge with a crack located at the position of $L/3$ from the left end is analyzed. The beam is divided by 50 elements. The boundary conditions at the two ends of the beam are as follows. At the left end: translations in the x, y, z directions and rotations about the x, y axes are fixed, while the rotation about the z axis is free. At the right end: the rotation about the z axis and the translation in the x direction are free, while translations in the y, z directions and rotations about the x, y axes are fixed. Parameters of the beam are: Mass density is 7800 kg/m^3; modulus of elasticity $E = 2.1 \times 10^{11}$ N/m^2; $L = 50$ m; $b = 1$ m; $h = 2$ m. In order to investigate the influence of the crack depth on the mode shapes of the beam four levels of the crack from zero to 30% are applied. These four cases are numbered as in Tab. 1.

Table 1. Four cases with cracks of varying depths

Case	Crack depth (%)
1	0
2	10
3	20
4	30

The mode shapes are plotted in 3D views by using the values of the three translation degrees of freedom in the x, y and z directions of the eigenvector. The first mode shape of

the beam bridge with four different levels of crack depth is investigated and presented in Figs. 2 to 5. For the intact beam bridge, the first mode shape corresponds to the bending vibration in the y-direction. This mode shape is a plane curve and lies in the x-y plane, thus its projection on the x-z plane is parallel to the x-axis as can be seen from Fig. 2.

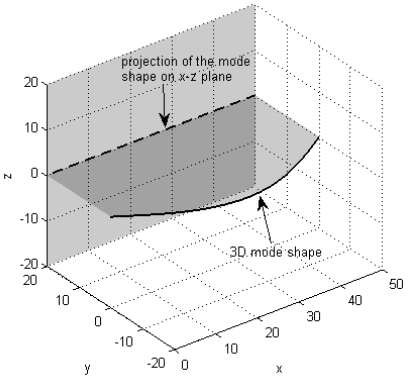

Fig. 2. The first mode shape, crack depth is 0%

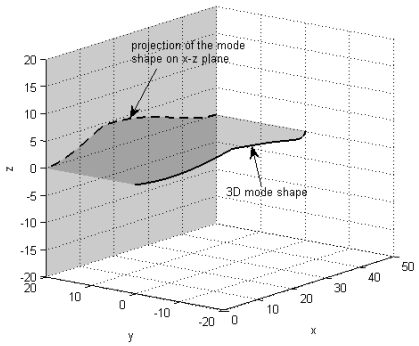

Fig. 3. The first mode shape, crack depth is 10%

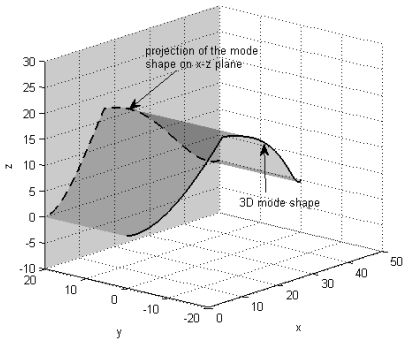

Fig. 4. The first mode shape, crack depth is 20%

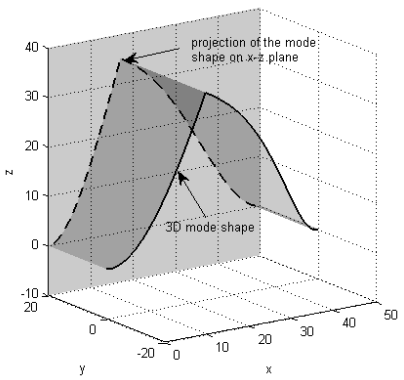

Fig. 5. The first mode shape, crack depth is 30%

In this case, the plane curve mode shape means the mode shape lies on a plane. The first mode shape obtained from the 3D crack model lying on the x-y plane corresponds to the first mode shape obtained from the 2D crack model. It is interesting to notice that, when there is a crack the first mode shape is slightly inclined from the x-y plane in the z direction. By amplifying appropriately the magnitude of the mode shape in the z-direction this incline can be seen clearly. The first mode shape amplified in the z-direction is presented in Fig. 3. The mode shape becomes a space curve and its projection on the x-z plane is not parallel to the x-axis as can be seen from this figure. The space curve mode shape means the mode shape does not lie on any plane but it twits in the space. When

the crack depth increases, the incline from the x-axis of the projection of mode shape on the x-z plane increases as presented in Figs. 4 and 5.

It can be observed that the projection of the first mode shape on the x-z plane has a sharp change at the crack position. In order to investigate the influence of the crack depth on the first mode shape, the projections of the mode shape with different levels of crack depth are presented in the same graph. Four projections of the first mode shape with four different levels of the crack depth are presented in Fig. 6. As can be seen from this figure, the projections of mode shape on the x-z plane have sharp changes at the location of $L/3$ which corresponds to the crack position. When the crack depth increases, the incline of the projection of the mode shape with respect to the x-axis increases. From these observations it is concluded that when there is a crack the first mode shape will be inclined from the x-y plane. The position at which the projection of mode shape on the x-z plane has a sharp change corresponds to the crack location. Thus, the projection of the first mode shape can be used to detect the crack existence and the crack position. The existence of the crack is indicated by the change of the first mode shape from the plane curve to the space curve. The crack position can be determined by the location at which the projection of the first mode shape on the x-z plane has a sharp change.

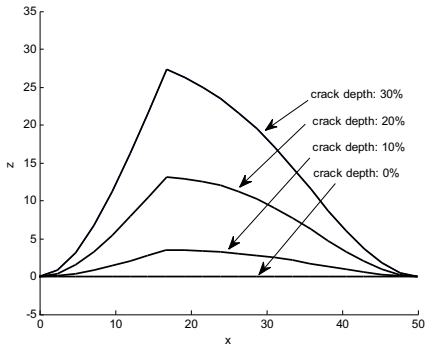

Fig. 6. Projections of the first mode shape on the x-z plane with four levels of crack depth

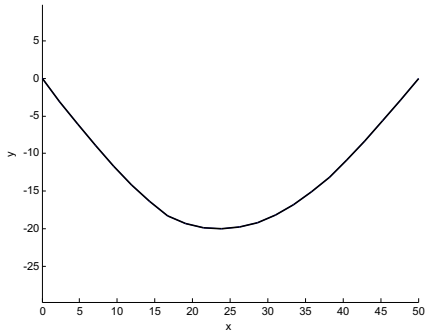

Fig. 7. Projections of the first mode shape on the x-y plane with crack depth of 30%

The change of the first mode shape from the plane curve to the space curve can be explained by the coupling phenomenon between the horizontal and vertical bending vibrations caused by the 3D crack. Since the sliding effect can be ignored in front of the bending effect as discussed in [13], the coupling between horizontal bending and vertical bending depends mainly on the bending effect of the crack. Numerical simulation has been carried out to show that the bending vibration of the beam with a 3D crack is the same with that of beam with a 2D crack when the coupling mechanism is disregarded.

The projection of the first mode shape on the x-y plane of the beam with the crack depth of 30% is presented in Fig. 7 to compare to the 2D crack model. No distortion in this projection of the mode shape can be seen at the crack location. This is similar to previous results where 2D crack models were applied [17, 18]: distortions in the mode shapes due to the crack cannot be seen visually with a small crack depth, it can only be seen with a very large crack depth. This implies that the projection of the first mode

shape on the x-y plane which corresponds to the 2D crack model cannot be used directly for crack detection when the crack depth is small.

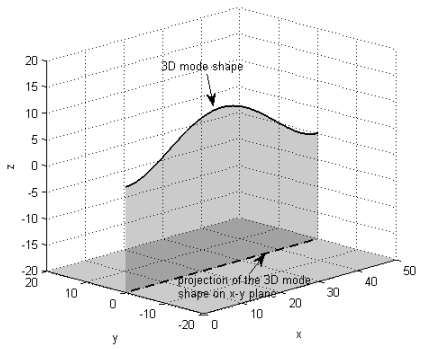

Fig. 8. The second mode shape, crack depth is 0%

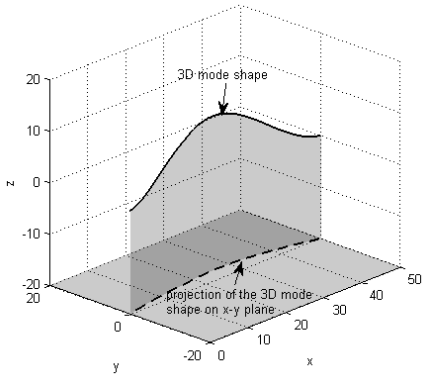

Fig. 9. The second mode shape, crack depth is 10%

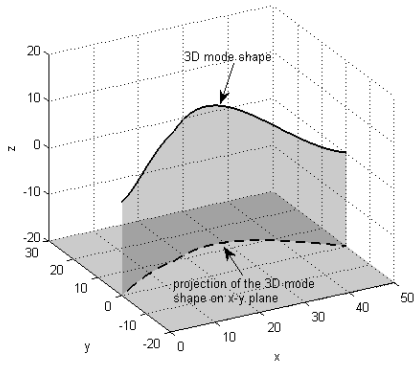

Fig. 10. The second mode shape, crack depth is 20%

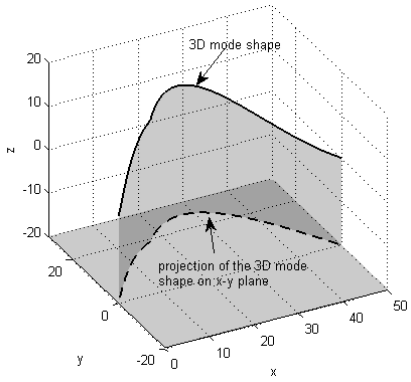

Fig. 11. The second mode shape, crack depth is 30%

Figs. from 8 to 13 present the second mode shapes with four levels of crack depth. When the crack depth is zero, the second mode shape is a plane curve lying on the x-z plane and its projection on the x-y plane is parallel to the x-axis as can be seen in Fig. 8. When there is a crack, the projection of the second mode shape on the x-y plane is not parallel to the x-axis anymore but it inclines from this axis as can be observed from Figs. 9 to 12. A small distortion of the mode shape in the 3D view and in the projection of the mode shape at the crack position can also be seen from these figures. However, this distortion of the mode shape is not as clear as the first mode shape. Moreover, no distortion can be found in the projection of this mode shape on the x-z plane with a crack depth of up to 30% which corresponds to the 2D crack model as presented in Fig. 13. Thus, the projection of the second mode shape on the x-y plane is only useful for detecting the

existence of the crack. The second mode shape and its projection on the x-y plane are not useful for determining the position of the crack.

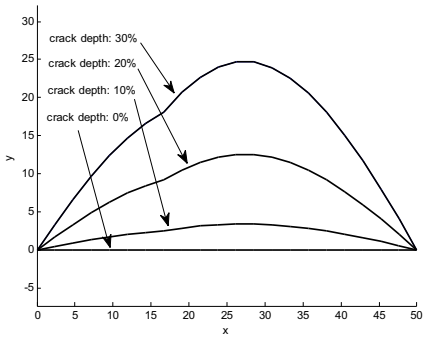

Fig. 12. Projections of the second mode shape on the x-y plane with four levels of crack depth

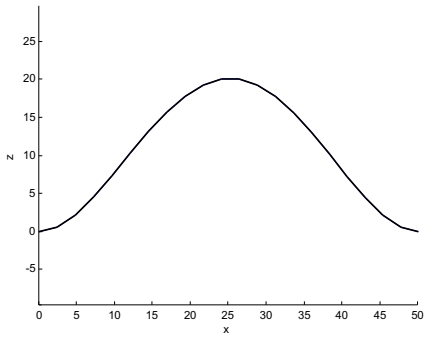

Fig. 13. Projections of the second mode shape on the x-z plane with crack depth of 30%

The third mode shape is presented in Figs. 14 to 19. When the crack depth is zero, the third mode shape is a plane curve lying on the x-z plane and its projection on the x-y plane is parallel to the x axis as can be seen in Fig. 14. When there is a crack, the third mode shape inclines from the x-z plane in the y-direction. The projection of the third mode shape on the x-y plane inclines from the x-axis as can be observed from Figs. 15 to 17. The distortion of the mode shape in the 3D view at the crack position can also be seen from these figures. This distortion can be seen clearer by projecting the mode shape on the x-y plane as shown in Fig. 18. It is evident a sharp change in the projection of the third mode shape can be detected at the crack location, while no distortion can be detected in the projection of the mode shape in the x-z plane as shown in Fig. 19.

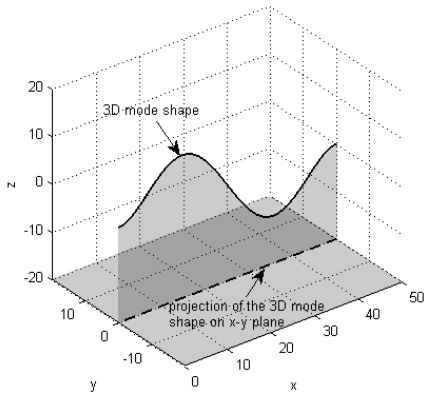

Fig. 14. The third mode shape, crack depth is 0%

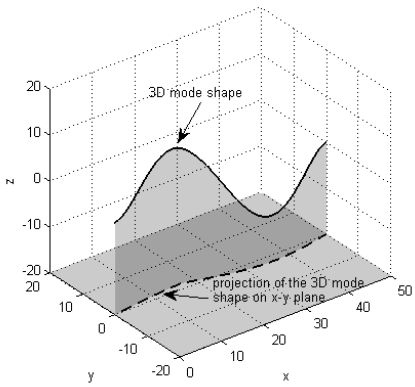

Fig. 15. The third mode shape, crack depth is 10%

From the above discussion, it can be said that all of the first three mode shapes can be used for detection of the crack existence. However, while the first and the third mode

shapes are useful for detection of the crack location, it is difficult to use the second mode shape for the same purpose.

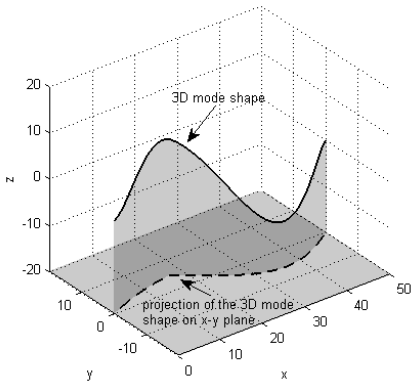

Fig. 16. The third mode shape, crack depth is 20%

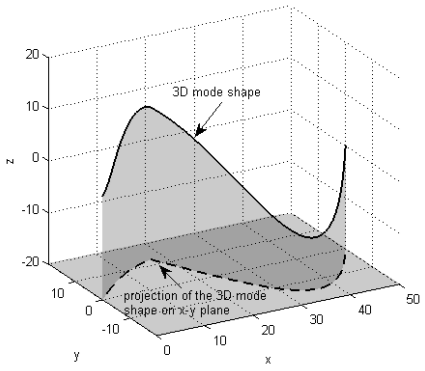

Fig. 17. The third mode shape, crack depth is 30%

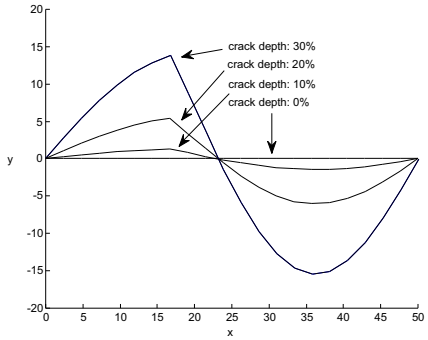

Fig. 18. Projections of the third mode shape on the x-y plane with four levels of crack depth

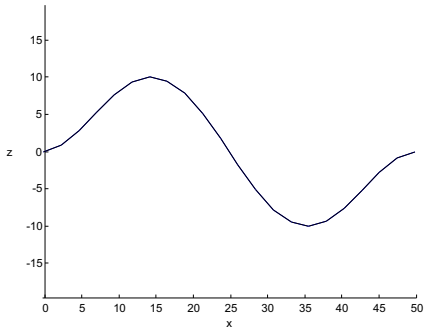

Fig. 19. Projections of the third mode shape on the x-z plane with crack depth of 30%

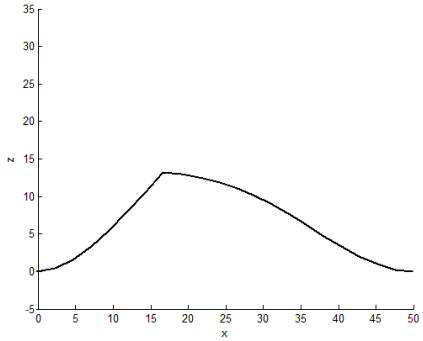

Fig. 20. Projection of the first mode shape, crack depth is 1%

It should be noted that, in order to compare the influence of the different levels of crack depth on the mode shapes in the same graph with the same scale, only three levels of crack depth ranging from 10% to 30% are investigated in this paper as presented above. However, smaller cracks can still be detected by the applying the mode shapes to larger scales. Fig. 20 presents the projection of the first mode shape on the x-z plane with the crack depth of 1% amplified to a scale which is two hundred times larger than the normalized scale. It is evident a sharp change in the projection of the third mode shape can be detected clearly at the crack location. This means that the proposed method can be applied for detection arbitrary small cracks by amplifying the mode shapes to appropriate scales.

5. SUMMARY AND CONCLUSION REMARKS

In this paper, the mode shapes of a 3D cracked beam-like bridge are calculated using finite element method. The twist of mode shapes caused by a 3D crack can be applied for crack detection of a beam-like bridge. The derivation of the stiffness matrix of a 3D cracked element derived from fracture mechanics is presented. The concluding remarks can be listed as follows:

It is interesting to notice that, due to the coupling mechanism of the 3D crack model, the mode shapes become space curves instead of plane curves. The mode shape in the 3D model inclines from its plane which corresponds to the case of intact beam.

Therefore, the existence of the crack can be determined by the incline of the mode shape from its plane in the case of intact beam or the mode shapes change from plane curve to space curves.

The position of distortions or sharp changes in the mode shapes caused by the crack can be determined as the position of the crack.

The advantage of using the 3D crack model over the 2D crack model is that the influence of crack on the mode shapes can be observed visually with arbitrary small crack depth by amplifying the mode shapes to appropriate scales. In this paper, the detection of a crack with depth as small as 1% is presented, while in previous studies using 2D crack models, the distortion of crack can only be inspected from the mode shape with a crack depth of lager than 50% [17, 18]. This result is new and can be applied for crack detection of a beam.

ACKNOWLEDGEMENTS

This paper was sponsored by the Vietnam National Foundation for Science and Technology Development (NAFOSTED) 2011-2013.

REFERENCES

[1] T. Chondros, A. Dimarogonas, and J. Yao. A continuous cracked beam vibration theory. *Journal of Sound and Vibration*, **215**(1), (1998), pp. 17–34.

[2] Y.-S. Lee and M.-J. Chung. A study on crack detection using eigenfrequency test data. *Computers & structures*, **77**(3), (2000), pp. 327–342.

[3] S. Orhan. Analysis of free and forced vibration of a cracked cantilever beam. *Ndt & E International*, **40**(6), (2007), pp. 443–450.

[4] P. Gudmundson. Eigenfrequency changes of structures due to cracks, notches or other geometrical changes. *Journal of the Mechanics and Physics of Solids*, **30**, (5), (1982), pp. 339–353.

[5] W. Zhang, Z. Wang, and H. Ma. Crack identification in stepped cantilever beam combining wavelet analysis with transform matrix. *Acta Mechanica Solida Sinica*, **22**(4), (2009), pp. 360–368.

[6] J. A. Loya, L. Rubio, and J. Fernández-Sáez. Natural frequencies for bending vibrations of timoshenko cracked beams. *Journal of sound and vibration*, **290**(3), (2006), pp. 640–653.

[7] S. Neild, P. Mcfadden, and M. Williams. A discrete model of a vibrating beam using a time-stepping approach. *Journal of sound and vibration*, **239**(1), (2001), pp. 99–121.

[8] E. Douka, G. Bamnios, and A. Trochidis. A method for determining the location and depth of cracks in double-cracked beams. *Applied Acoustics*, **65**(10), (2004), pp. 997–1008.

[9] N. Khaji, M. Shafiei, and M. Jalalpour. Closed-form solutions for crack detection problem of timoshenko beams with various boundary conditions. *International Journal of Mechanical Sciences*, **51**, (9), (2009), pp. 667–681.

[10] K. V. Nguyen. Comparison studies of open and breathing crack detections of a beam-like bridge subjected to a moving vehicle. *Engineering Structures*, **51**, (2013), pp. 306–314.

[11] C. Papadopoulos and A. Dimarogonas. Coupled longitudinal and bending vibrations of a rotating shaft with an open crack. *Journal of Sound and Vibration*, **117**(1), (1987), pp. 81–93.

[12] A. Darpe, K. Gupta, and A. Chawla. Coupled bending, longitudinal and torsional vibrations of a cracked rotor. *Journal of Sound and Vibration*, **269**(1), (2004), pp. 33–60.

[13] P. Saavedra and L. Cuitino. Crack detection and vibration behavior of cracked beams. *Computers & Structures*, **79**(16), (2001), pp. 1451–1459.

[14] S. Quek and G. Liu. *Finite Element Method: A Practical Course: A Practical Course*. Butterworth-Heinemann, (2003).

[15] H. Tada, P. C. Paris, and G. R. Irwin. *The stress analysis of cracks handbook*, Vol. 130. ASME press New York, (2000).

[16] J. Lee. Identification of multiple cracks in a beam using natural frequencies. *Journal of sound and vibration*, **320**(3), (2009), pp. 482–490.

[17] P. Rizos, N. Aspragathos, and A. Dimarogonas. Identification of crack location and magnitude in a cantilever beam from the vibration modes. *Journal of sound and vibration*, **138**(3), (1990), pp. 381–388.

[18] S. Caddemi and I. Caliò. The exact explicit dynamic stiffness matrix of multi-cracked euler–bernoulli beam and applications to damaged frame structures. *Journal of Sound Vibration*, **332**, (2013), pp. 3049–3063.

VIETNAM ACADEMY OF SCIENCE AND TECHNOLOGY
VIETNAM JOURNAL OF MECHANICS VOLUME 36, N. 1, 2014

CONTENTS